

High-energy electron-impact excitation process: The generalized oscillator strengths of helium

Xiao-Ying Han^{1,*} and Jia-Ming Li^{2,1,†}¹Key Laboratory of Atomic and Molecular Nanosciences of Education Ministry, Department of Physics, Tsinghua University, Beijing 100084, China²Department of Physics, Shanghai Jiao Tong University, Shanghai 200230, China

(Received 21 June 2006; published 18 December 2006)

The high-energy electron impact excitation cross sections are directly proportional to the generalized oscillator strengths (GOSs) of the target (an atom or molecule). In the present work, the GOSs of helium from the ground state to n^1S , n^1P , n^1D ($n \rightarrow \infty$) and adjacent continuum excited states are calculated by a modified R -matrix code within the first Born approximation. In order to treat the bound-bound and bound-continuum transitions in a unified manner, the GOS density (GOSD) is defined based on the quantum defect theory. The GOSD surfaces of 1S , 1P , and 1D channels are calculated and tested stringently by the recent experiments. With the recommended GOSD surfaces with sufficient accuracy, the GOSDs (i.e., GOSs) from the ground state into all n^1S , n^1P , and n^1D excited states of helium can be obtained by interpolation. Thus, the high-energy electron impact excitation cross sections of all these excited states can be readily obtained. In addition to the high-energy electron impact excitation cross sections, a scheme to calculate the cross sections in the entire incident energy range is discussed.

DOI: 10.1103/PhysRevA.74.062711

PACS number(s): 34.80.Dp, 31.15.-p, 32.70.Cs, 34.50.Fa

I. INTRODUCTION

Electron impact excitation processes are important in diverse fields such as radiation physics, plasma physics, atmospheric physics, and astrophysics. With ever-increasing needs, such cross-section data are indispensable physical parameters in the above-mentioned fields. In an electron impact excitation process, the target (an atom or molecule) can be excited into all sorts of excited states, e.g., an infinite number of Rydberg, autoionization, and continuum states, as long as the process satisfies the energy and momentum conservations. The differential scattering cross section is a function of the incident energy E_i , the energy transfer ΔE , and the scattering angle Ω of the impact electron. Since the scattering angle is equivalent to the momentum transfer \vec{K} in describing the collision process, the scattering angle is substituted by the momentum transfer for convenience. If the incident energy of the impact electron is high enough but still nonrelativistic, the first Born approximation (FBA) is applicable and the incident and scattered electrons can be treated as plane waves. Within the FBA, the expression of the differential cross section (DCS) consists of two distinct parts: one only deals with the incident electron, which is a trivial factor; the other deals with the target, which is the generalized oscillator strength (GOS) and is independent of the incident energy [1–6]. Therefore, the DCS is proportional to the GOS, which is a function of the momentum transfers K and the energy transfers ΔE . In the limit of zero momentum transfer, the GOS becomes equal to the optical oscillator strength. This connects the high-energy electron impact excitation process with the photoabsorption or photoionization processes.

In the framework of the quantum defect theory (QDT) [7–10], all the infinite excited states, including Rydberg and

adjacent continuum states, can be classified as channels; e.g., for helium, in the 1P channel, there are infinite n^1P ($2 \leq n < \infty$) and adjacent ε^1P continuum states. The physical parameters of such channels (e.g., the quantum defects μ_α and the transformation matrix $U_{i\alpha}$) are smooth functions of the excitation energies [7–10]. In the R -matrix method [11–17], the initial- and final-state wave functions are expanded on equal footing. Using a modified R -matrix code, the GOSs of the target can be calculated by evaluating the transition matrix elements between the initial and final states. In order to treat the bound-bound and bound-continuum transitions in a unified manner, the GOS density (GOSD) is defined [2–6], which is a smooth function of the excitation energies in a channel. The GOSD curves of the excited states in a channel form a surface, which is a smooth function of the momentum transfers and the excitation energies. In our previous work [5], we reported the preliminary calculation results of helium by the modified R -matrix code, which were only compared with the previous experimental results [18]. In this work, we will present more detailed descriptions of the method and make a detailed comparison with the recent experimental results [19], which will give a more stringent test of the theoretical method by this simple and nontrivial prototype system. Recently, Liu *et al.* [19] measured the absolute GOSs of the excited states 2^1S , 3^1S , 4^1S , 2^1P , 3^1P+3^1D , 4^1P+4^1D , $5^1S+^1P+5^1D$, and $6^1S+^1P+6^1D$ for helium at the incident energy 2500 eV with the energy resolution 80 meV [full width at half-maximum (FWHM)] in the momentum transfer range $0.07 \leq K^2 \leq 3.6$ a.u. The absolute measurements with such high resolutions provide the benchmark experiments to test the theoretical method and the modified code stringently.

Using the modified R -matrix code, the GOSs of helium from the ground state to n^1S , n^1P , and n^1D ($n \rightarrow \infty$) and adjacent continuum excited states are calculated within the FBA. For n^1S ($n=2,3,4$) and 2^1P , excited states, our calculated GOSs agree with the recent high-energy experimen-

*Electronic address: hanxiaoying@tsinghua.org.cn

†Electronic address: lijm@sjtu.edu.cn

tal results [19]. For the excited states with high principal quantum numbers, e.g., n^1P+n^1D ($n=3,4$) and $n^1S+n^1P+n^1D$ ($n=5,6$), the GOSs are measured as a whole and cannot be resolved experimentally because of the energy resolution limit. For these states, our calculated total GOSs agree with the unresolved experimental results within the experimental uncertainties. Although there are no resolved experimental GOSs of n^1D excited states, which are smaller than those of the corresponding n^1S states but with the same order of magnitude, our calculated GOSs of n^1D states are anticipated to have the same accuracy as those of n^1S states since all the excited-state wave functions are expanded on equal footing in the R -matrix method. More specifically, since the GOSs of n^1P states are larger than the GOSs of corresponding n^1D and n^1S states by about one or two orders, the experimental GOSs of n^1P ($n=3,4,5,6$) states can be separated from the unresolved experimental total GOSs by subtracting the corresponding theoretical GOSs of n^1D and n^1S states. The available experimental GOSs of n^1P ($n=2,3,4,5,6$) states can be used to examine the GOSD surface of the 1P channel. Note that the GOSD surface can be calculated based on a few GOSD curves of the bound and adjacent continuum states in an efficient way. In this work, the GOSD surfaces of 1S , 1P , and 1D channels are calculated and examined by the available experimental values. With the recommended GOSD surfaces of sufficient accuracy, the GOSDs (i.e., GOSs) of all n^1S , n^1P , and n^1D excited states can be obtained by interpolation instead of laborious *ab initio* calculations. Since the high-energy electron impact excitation differential cross sections (DCSs) are proportional to the GOSs, the DCSs of these excited states can be readily obtained. This can satisfy the ever-increasing needs of various relevant fields. In addition to the high-energy electron impact excitation process, a scheme to deal with the cross sections in the entire energy range, including low and intermediate energy, is discussed in Sec. III. Similarly to the GOS, the apparent GOS (AGOS) for the low- and intermediate-energy impact processes can be defined, which is a function of the incident energies E_i in addition to the energy transfers ΔE and the momentum transfers K . The corresponding apparent GOSD (AGOSD) can also be defined. The AGOSD for the intermediate-energy electron impact process is anticipated to be a smooth function of the excitation energies and the momentum transfers at various given incident energies, e.g., forming sets of smooth surfaces in ΔE and K spaces. However, at low incident energies, the assumption that the AGOSD is a smooth function of ΔE and K is not valid because of the involvement of only a few partial amplitudes and the existence of resonances.

II. THEORETICAL METHODS AND RESULTS

In an electron impact excitation process, the differential cross section $d\sigma/d\Omega$ is equal to $\frac{k'}{k}|f(\hat{k}')|^2$ (in atomic units). Here $f(\hat{k}')$ is the scattering amplitude, which can be calculated by the following formula [20]:

$$\begin{aligned} f(\hat{k}') &= -\frac{1}{2\pi} \langle e^{i\vec{k}' \cdot \vec{r}} \chi', \varphi_{T'}(\tilde{L}' \tilde{S}' \tilde{\pi}') | V(\vec{r}_1 \cdots \vec{r}_N, \vec{r}) | \Psi^+ \rangle \\ &= -\frac{1}{2\pi} \langle e^{i\vec{k}' \cdot \vec{r}} \chi', \varphi_{T'}(\tilde{L}' \tilde{S}' \tilde{\pi}') | T | e^{i\vec{k} \cdot \vec{r}} \chi, \varphi_T(\tilde{L} \tilde{S} \tilde{\pi}) \rangle \\ &= \sum_{LS\pi} f_{LS\pi}(\hat{k}'), \end{aligned} \quad (1)$$

where T is the transition matrix. \vec{k} (\vec{k}') and χ (χ') are, respectively, the wave vector and spin wave function of the initial (final) state of the impact electron. $\varphi_T(\tilde{L} \tilde{S} \tilde{\pi})$ and $\varphi_{T'}(\tilde{L}' \tilde{S}' \tilde{\pi}')$ are the initial- and final-state wave functions of the target with the definite angular momentum \tilde{L} (\tilde{L}'), spin \tilde{S} (\tilde{S}') and parity $\tilde{\pi}$ ($\tilde{\pi}'$). The wave function $|e^{i\vec{k} \cdot \vec{r}} \chi, \varphi_T(\tilde{L} \tilde{S} \tilde{\pi})\rangle$ for the $(N+1)$ -electron system including the impact electron and the target has the following normalization condition: $\langle e^{i\vec{k} \cdot \vec{r}} \chi, \varphi_T(\tilde{L} \tilde{S} \tilde{\pi}) | e^{i\vec{k}' \cdot \vec{r}} \chi', \varphi_{T'}(\tilde{L}' \tilde{S}' \tilde{\pi}') \rangle = (2\pi)^3 \delta_{TT'} \delta(\vec{k} - \vec{k}') = (2\pi)^3 \delta_{TT'} \frac{1}{k} \delta(k - k') \delta(\epsilon - \epsilon')$; here $\epsilon = k^2/2$. $V(\vec{r}_1 \cdots \vec{r}_N, \vec{r})$ is the interaction operator between the impact electron and the target, which is equal to $\sum_{\alpha=1}^N \frac{-1}{|\vec{r} - \vec{r}_\alpha|} + \frac{Z}{r}$ (Z is the charge of the atomic nucleus) if the interaction is Coulombic. N is the number of the electrons in the target. \vec{r} and \vec{r}_α are, respectively, the coordinates of the impact electron and the α th electron in the target relative to the centroid of the target. The wave function $\Psi^+(\vec{r}_1 \cdots \vec{r}_N, \vec{r})$ characterizes the asymptotic behavior of the initial state for the $(N+1)$ -electron system. The partial scattering amplitude $f_{LS\pi}(\hat{k}')$ is

$$\begin{aligned} f_{LS\pi}(\hat{k}') &= -\frac{\pi}{\sqrt{k'k}} \sum_{ij} \sum_{m_l m_s} \sum_{m_s} \sum_{\tilde{M} \tilde{L} \tilde{S} \tilde{\pi}} \sum_{\tilde{M}' \tilde{L}' \tilde{S}' \tilde{\pi}'} \sqrt{4\pi(2l_i + 1)} \\ &\quad \times Y_{l_j m_j}(\hat{k}') T_{ji}^{LS\pi} \times \langle \tilde{L}' \tilde{M}'_{\tilde{L}'} l_j m_j | LM_L \rangle \\ &\quad \times \langle \tilde{S}' \tilde{M}'_{\tilde{S}'} s_j m_s | SM_S \rangle \langle LM_L | \tilde{L} \tilde{M}_{\tilde{L}} l_i 0 \rangle \\ &\quad \times \langle SM_S | \tilde{S} \tilde{M}_{\tilde{S}} s_i m_s \rangle. \end{aligned} \quad (2)$$

For convenience, the direction of \vec{k} is defined as the \hat{z} axis. i and j are the channel labels, i.e., $i(l_i; \tilde{L} \tilde{S} \tilde{\pi})$ and $j(l_j; \tilde{L}' \tilde{S}' \tilde{\pi}')$; l_i (l_j) and s_i (s_j) are the angular momentum and spin of the impact (scattered) electron. The total angular momentum L , spin S , and parity π of the $(N+1)$ -electron system are good quantum numbers in an electron impact process. $T_{ji}^{LS\pi}$ are the reduced transition matrix elements in $LS\pi$ representation, which only connect the initial and final states with the same $LS\pi$ because of the conservation of the good quantum numbers. Moreover, $T_{ji}^{LS\pi}$ are independent of the magnetic quantum numbers because of the rotational invariance of the scattering interaction. According to Bethe theory [1,21], if the incident energy of the impact electron is high enough, Ψ^+ is equal to $|e^{i\vec{k} \cdot \vec{r}} \chi, \varphi_T(\tilde{L} \tilde{S} \tilde{\pi})\rangle$ within the FBA [1,2], and the amplitude is

$$\begin{aligned}
f^B(\hat{k}') &= -\frac{1}{2\pi} \langle e^{i\vec{k}' \cdot \vec{r}} \chi', \varphi_{T'}(\tilde{L}' \tilde{S}' \tilde{\pi}') | V | e^{i\vec{k} \cdot \vec{r}} \chi, \varphi_T(\tilde{L} \tilde{S} \tilde{\pi}) \rangle \\
&= -\frac{2}{K^2} \langle \varphi_{T'}(\tilde{L}' \tilde{S}' \tilde{\pi}') | \sum_{\alpha=1}^N e^{i\vec{k} \cdot \vec{r}_\alpha} | \varphi_T(\tilde{L} \tilde{S} \tilde{\pi}) \rangle \\
&= \sum_{LS\pi} f_{LS\pi}^B(\hat{k}'), \tag{3}
\end{aligned}$$

where $f^B(\hat{k}')$ is the Born scattering amplitude. In the second line of Eq. (3), the coordinate \vec{r} of the impact electron is integrated as a whole [1,2]. $\vec{K} = \vec{k} - \vec{k}'$ is the momentum transfer of the impact electron. The Born partial scattering amplitude $f_{LS\pi}^B(\hat{k}')$ can be calculated by Eq. (2), where the reduced transition matrix should be the Born reduced transition matrix $T_{ji}^{LS\pi(B)}$ calculated within the FBA. Note that the above expression for the Born scattering amplitude consists of two parts: one only deals with the impact electron, which is nearly a trivial number factor; the other part deals with the target, which is defined as the GOS of the target [1–6],

$$\begin{aligned}
F(\Delta E, K) &= \frac{2\Delta E}{K^2} \left| \langle \varphi_{T'}(\tilde{L}' \tilde{S}' \tilde{\pi}') | \sum_{\alpha=1}^N e^{i\vec{k} \cdot \vec{r}_\alpha} | \varphi_T(\tilde{L} \tilde{S} \tilde{\pi}) \rangle \right|^2 \\
&= \frac{K^2 \Delta E}{2} |f^B(\hat{k}')|^2, \tag{4}
\end{aligned}$$

where ΔE is the energy transfer. Therefore, the DCS at high incident energy is proportional to the GOS within the FBA,

$$\frac{d\sigma}{d\Omega} = \frac{k'}{k} |f^B(\hat{k}')|^2 = \frac{2}{\Delta E} \frac{k'}{k} \frac{F(\Delta E, K)}{K^2}. \tag{5}$$

In the limit of zero momentum transfer, the GOS becomes equal to the optical oscillator strength [1–6]. This connects the high-energy electron impact excitation process with the photoabsorption or photoionization processes.

The GOS can be calculated by the R -matrix method according to Eq. (4). Since the detailed descriptions of the R -matrix method have been presented in the previous works [11–17], here only a brief outline will be given. In the R -matrix method, the initial- and final-state wave functions (φ_T and $\varphi_{T'}$) are expanded on equal footing. This method begins by partitioning the subconfiguration space of the excited electron into two regions by a sphere of radius a centered on the nucleus. In the external region ($r \geq a$), where r is the distance of the excited electron relative to the centroid of the core, the exchange interactions between the excited electron and the core electrons are negligible if the radius a is chosen to be large enough so that the charge distribution of the core is restricted in the sphere. In the external region, the excited electron mainly “feels” the Coulomb potential as well as the long-range static polarization potential. Thus the outer region wave functions of the excited electron can be expanded by regular and irregular Coulomb wave functions analytically, which satisfy the boundary conditions at infinity [22].

Within the reaction zone ($r \leq a$), the interactions between the excited electron and the core electrons involve electron exchange and correlation interactions. This is a many-body problem and solved variationally as a whole to obtain the logarithmic derivative boundary matrix $\mathfrak{R}(E)$ on the R -matrix box surface (i.e., $r=a$). Therefore, within the reaction zone the electron correlations for the N -electron system including the core and the excited electron are calculated adequately by the variational method [22,23]. Within this region, the wave functions Ψ of eigenenergy E for the N -electron system are expanded as

$$\Psi = \sum_k A_{Ek} \Psi_k. \tag{6}$$

Here Ψ_k are a set of energy-independent configuration bases, which are expanded as

$$\begin{aligned}
\Psi_k &= \mathcal{A} \sum_{ij} a_{ijk} \tilde{\Phi}_i(\vec{r}_1 \cdots \vec{r}_\alpha \cdots \vec{r}_{N-1}; \hat{r}_N, \sigma_N) \frac{1}{r_N} u_{ij}(r_N) \\
&\quad + \sum_j b_{jk} \phi_j(\vec{r}_1 \cdots \vec{r}_\alpha \cdots \vec{r}_N), \tag{7}
\end{aligned}$$

where \mathcal{A} is the antisymmetrization operator which accounts for the electron exchanges between the core electrons and the excited electron; \vec{r}_α is the coordinate of the α th electron in the core; u_{ij} is the continuum orbital bases; ϕ_j is completely formed by the bound orbitals to ensure the completeness of the wave functions for the N -electron system and takes account of the electron correlations within the reaction zone; and $\tilde{\Phi}_i$, which has definite total angular momentum and parity, is the i th channel wave function obtained by coupling the core wave functions with the angular and spin wave functions of the N th electron. More specifically, the core wave functions are usually written as the linear superpositions of a set of basis configurations to take into account the electron correlations by a self-consistent multiconfiguration interaction method. These basis configurations are constructed as antisymmetrized product-type wave functions by a set of bound orbital bases with appropriate angular momentum couplings. The radial wave functions of these bound orbital bases are the linear superpositions of the Slater-type-orbital bases [24]. In the present work, we use the following set of orbital bases: $1s, 2s, 2p, 3s, 3p, 3d, \bar{4}s, \bar{4}p, \bar{4}d$, which are obtained by the variational method with the CIVPOL code [25–27]. Here $\bar{4}s, \bar{4}p, \bar{4}d$ are polarized pseudo-orbitals [25–27], which take account of the static polarization effects sufficiently. All the other orbitals $1s-3d$ are spectroscopic orbitals with $n-l-1$ nodes. Based on this set of orbital bases and carefully chosen nine target states arising from the configurations ($1snl; n \leq 4, l \leq 2$), the lowest ionization energy for the ground state of helium converges to 1.7911 Ry, which agrees well with the experimental value 1.8074 Ry [28] by about 0.9%.

For an atom or molecule, there exist infinite excited states including Rydberg and adjacent continuum states near the threshold. In the framework of the quantum defect theory (QDT) [7–10], the infinite excited states are classified as channels; e.g., for helium, in the 1S channel, there are infinite

n^1S ($1 \leq n < \infty$) and adjacent ε^1S continuum states. The energy of the bound state can be written as (in a.u. units)

$$E = I_\alpha - \frac{1}{2\nu^2} = I_\alpha - \frac{1}{2(n - \mu_\alpha)^2}. \quad (8)$$

n is the principal quantum number. μ_α is the quantum defect of the eigenchannel α . I_α is the ionization threshold of the eigenchannel. The physical wave function of total eigenenergy E for the whole system is the superpositions of eigenchannel wave functions,

$$\Psi = \sum_\alpha \Psi_\alpha \cdot A_\alpha r \xrightarrow{\infty} \sum_\alpha \left\{ \mathcal{A} \sum_i \Theta_i \cdot U_{i\alpha} [f_i(r, E) \cos(\pi\mu_\alpha) - g_i(r, E) \sin(\pi\mu_\alpha)] \right\} A_\alpha. \quad (9)$$

Here, Ψ_α are the eigenchannel wave functions. A_α are the mixing coefficients. \mathcal{A} is the antisymmetrization operator. The wave function Θ_i consists of the core state wave function combined with the angular and spin wave functions of the excited electron in the i th ionization channel. $U_{i\alpha}$ is the orthogonal transformation matrix. $f_i(r, E)$ and $g_i(r, E)$ are regular and irregular Coulombic wave functions, respectively. The physical parameters of eigenchannels, e.g., μ_α , $U_{i\alpha}$ and transition matrix elements (i.e., the scattering amplitudes), are smooth functions of the excitation energies. Reference [29] has elucidated how to calculate the eigenchannel wave functions and eigenchannel parameters of the multi-channel problem by the R -matrix method in detail. Here, for helium, it is a single-channel problem and its physical channel is the eigenchannel [29] (i.e., $\alpha=1$, $A_\alpha=1$, and $U_{i\alpha}$ is a unit matrix of one dimension). Therefore, its scattering amplitude in a channel (e.g., the 1P channel) is a smooth function of the excitation energy. In order to treat the bound-bound and bound-continuum transitions in a unified manner, the GOS density (GOSD) is defined as $dF(\Delta E, K)/dE$ (i.e., the generalized oscillator strengths per unit excitation energy) [2–6]. The GOS and GOSD have the following relation:

$$\left(\frac{dF_n(\Delta E, K)}{dE} \right)_\alpha = F_n(\Delta E, K) \frac{dn}{dE}, \quad (10)$$

where dn/dE stands for the density of state n . According to Eq. (8), $dn/dE = \nu^3 + d\mu_\alpha/dE$. Since μ_α is a smooth function of E , $d\mu_\alpha/dE$ is nearly zero.

Using the modified R -matrix code, we calculate the GOSs of helium from the ground state $[1s^2]^1S$ to n^1S , n^1P , and n^1D ($n \rightarrow \infty$) and adjacent continuum excited states. As shown in Figs. 1–4, our calculated GOSs of 2^1P and n^1S ($n=2, 3, 4$) excited states generally agree with the high-energy experimental results [18,19] by about 5%. However, for the 4^1S state, there are two experimental GOS points at $K^2=0.14$ and 0.23 deviating from our calculated smooth curve. Note that the GOS should be a smooth function of the momentum transfers and our calculated GOSs of the 4^1S state at smaller and larger K^2 agree with the experimental results, therefore the differences may result from the experi-

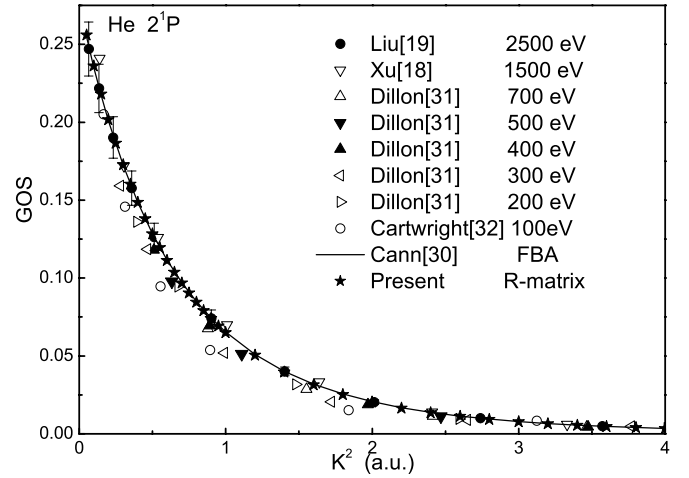


FIG. 1. The GOSs for the 2^1P excited state. (★) The present R -matrix calculation results; (—) the previous theoretical results of Ref. [30]; (●): the recent experimental results of Ref. [19] at 2500 eV incident energy; (Δ , ∇ , \blacktriangle , \blacktriangledown , \triangleleft , \triangleright , \circ) the previous experimental results [18,31,32] at lower incident energies: 100–1500 eV.

mental uncertainties, which deserve further experimental studies. Our calculated GOSs for these four excited states are larger than other experimental results [31–35] at lower incident energies, which will be discussed later. Our calculated GOSs agree well with the previous theoretical results of Cann *et al.* [30], which were calculated from the explicitly correlated wave functions within the FBA.

As shown in Figs. 1–4, the experimental GOSs at lower incident energies are close to and slightly lower than the GOSs at 2500 eV incident energy and the discrepancies reduce as the incident energies increase. This indicates the convergence of the FBA with the increasing incident energies. More specifically, as shown in Fig. 2, at small K^2 (nearly

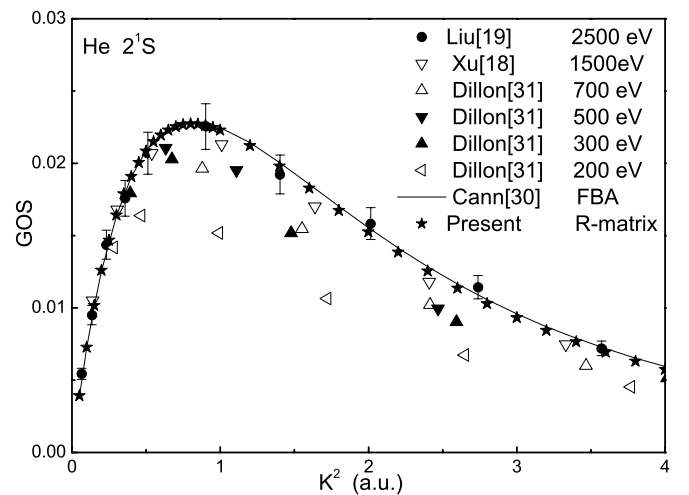


FIG. 2. The GOSs for the 2^1S excited state. (★) The present R -matrix calculation results; (—) the previous theoretical results of Ref. [30]; (●) the recent experimental results of Ref. [19] at 2500 eV incident energy; (Δ , ∇ , \blacktriangle , \blacktriangledown , \triangleleft) the previous experimental results [18,31] at lower incident energies: 200–1500 eV.

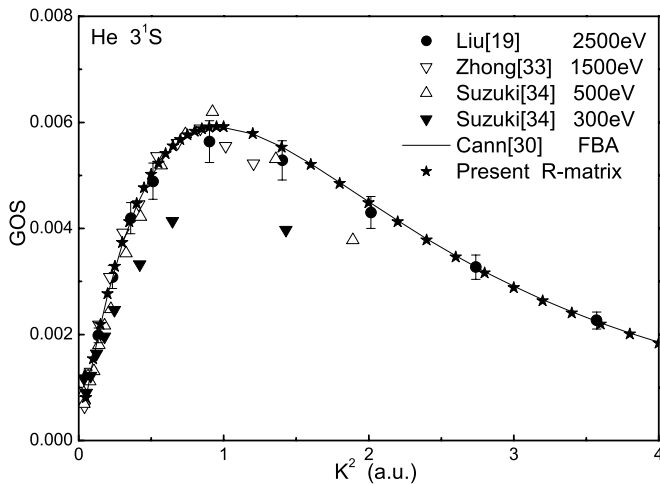


FIG. 3. The GOSs for the 3^1S excited state. (★) The present R-matrix calculation results; (—) the previous theoretical results of Ref. [30]; (●) the recent experimental results of Ref. [19] at 2500 eV incident energy; (Δ , ∇ , \blacktriangledown) the previous experimental results [33,34] at lower incident energies: 300–1500 eV.

equal to zero), the GOSs of Dillon at 200–700 eV incident energies agree with the GOSs of Liu at 2500 eV incident energy, and with increasing K^2 Dillon's results are smaller than Liu's results. This feature can be understood as follows. It is known that in the limit of zero momentum transfers the GOSs are equal to the optical oscillator strengths (OOSs). Therefore, at small K^2 the GOSs measured at different incident energies should converge to the same value (i.e., the OOSs). At larger K^2 , from a point of view of partial wave expansions, more and more partial wave contributions should be considered with increasing incident energies, until converging to the Born scattering amplitude. Therefore, the GOSs of Liu are greater than other measurements at larger K^2 .

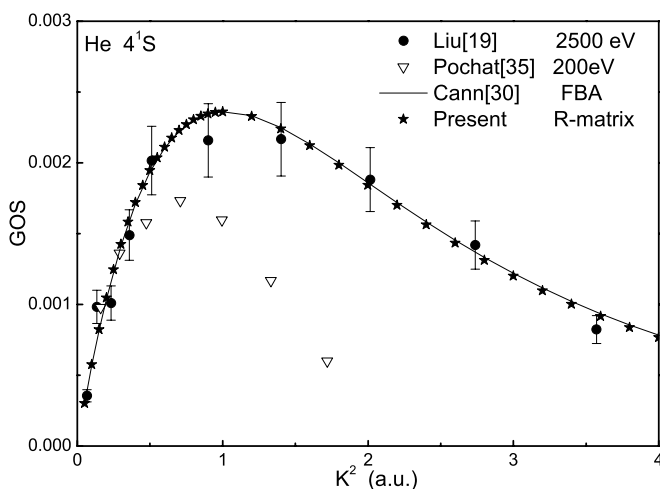


FIG. 4. The GOSs for the 4^1S excited state. (★) The present R-matrix calculation results; (—) the previous theoretical results of Ref. [30]; (●) the recent experimental results of Ref. [19] at 2500 eV incident energy; (∇) the previous experimental results [35] at 200 eV incident energy.

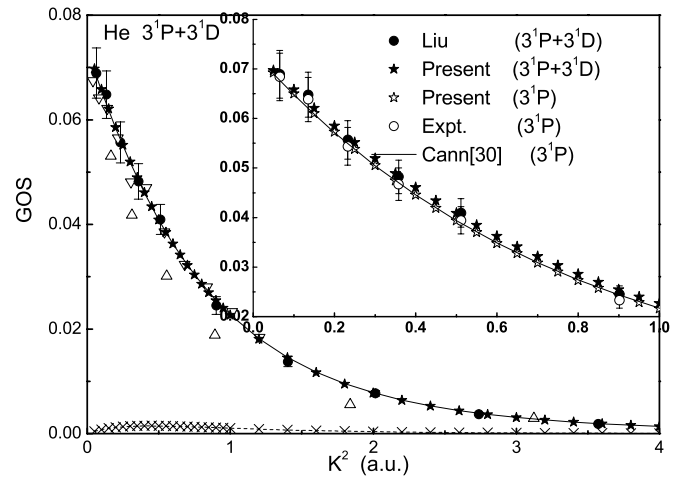


FIG. 5. The GOSs for 3^1P+3^1D excited states. (●) Experimental results of Ref. [19] at 2500 eV incident energy; (∇) experimental results of Ref. [33] at 1500 eV incident energy; (Δ) experimental results of Ref. [32] at 100 eV incident energy; (—) theoretical results of Ref. [30] for 3^1P+3^1D states; (—) theoretical results of Ref. [30] for the 3^1D state; (★) present calculated total GOSs for 3^1P+3^1D states; (\times) present calculated GOSs for the 3^1D state. Note that the experimental values (\circ) are obtained by subtracting the theoretical values (\times) from the experimental values (\bullet).

Because of the energy resolution limit, the GOSs of the excited states with high principal quantum numbers, e.g., n^1P+n^1D ($n=3,4$) and $n^1S+n^1P+n^1D$ ($n=5,6$), are measured as a whole and cannot be resolved experimentally. As shown in Figs. 5–8, our calculated total GOSs of n^1P+n^1D ($n=3,4$) and $n^1S+n^1P+n^1D$ ($n=5,6$) states agree with the unresolved high-energy experimental results [19] by about 5%, which is within the experimental uncertainties. It

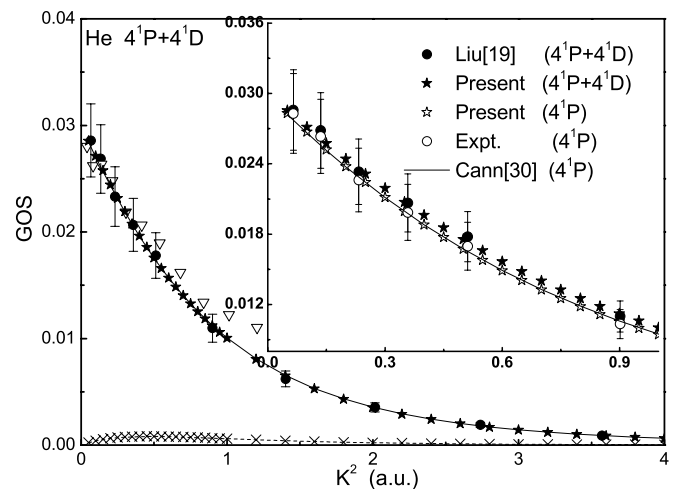


FIG. 6. The GOSs for 4^1P+4^1D excited states. (●) Experimental results of Ref. [19] at 2500 eV incident energy; (∇) experimental results of Ref. [33] at 1500 eV incident energy; (—) theoretical results of Ref. [30] for 4^1P+4^1D states; (—) theoretical results of Ref. [30] for the 4^1D state; (★) present calculated total GOSs for 4^1P+4^1D states; (\times) present calculated GOSs for the 4^1D state. The experimental values (\circ) are obtained by subtracting the theoretical values (\times) from the experimental values (\bullet).

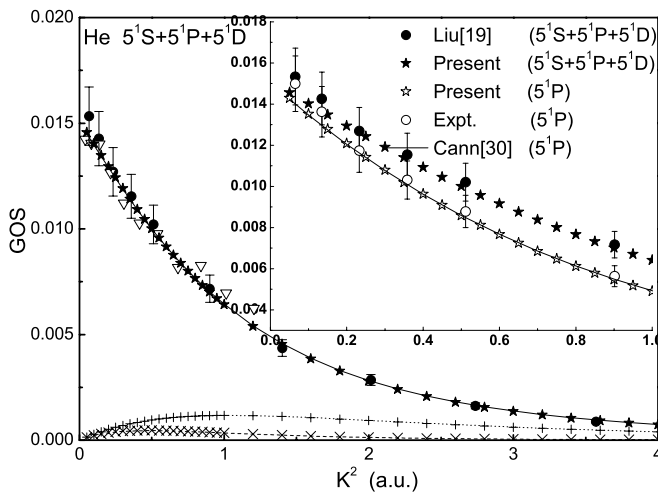


FIG. 7. The GOSs for $5^1S+5^1P+5^1D$ excited states. (●) Experimental results of Ref. [19] at 2500 eV incident energy; (▽) experimental results of Ref. [33] at 1500 eV incident energy; (–) theoretical results of Ref. [30] for $5^1S+5^1P+5^1D$ states; (···) theoretical results of Ref. [30] for the 5^1S state; (–) theoretical results of Ref. [30] for the 5^1D state; (★) present calculated total GOSs for $5^1S+5^1P+5^1D$ states; (+) present calculated GOSs for the 5^1S state; (×) present calculated GOSs for the 5^1D state. The experimental values (○) are obtained by subtracting the theoretical values (+) and (×) from the experimental values (●).

is noted that there are also two points of the experimental GOSs with $n=6$ at large K^2 deviating from our calculated smooth curve. The differences may also result from the experimental uncertainties with the same reason as that for the

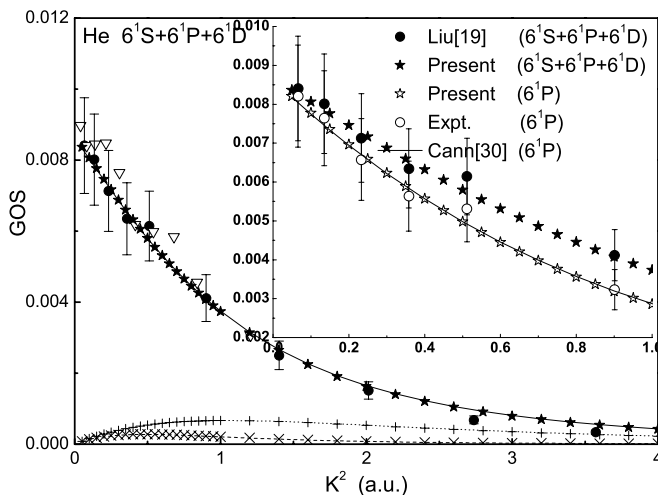


FIG. 8. The GOSs for $6^1S+6^1P+6^1D$ excited states. (●) Experimental results of Ref. [19] at 2500 eV incident energy; (▽) experimental results of Ref. [33] at 1500 eV incident energy; (–) theoretical results of Ref. [30] for $6^1S+6^1P+6^1D$ states; (···) theoretical results of Ref. [30] for the 6^1S state; (–) theoretical results of Ref. [30] for the 6^1D state; (★) present calculated total GOSs for $6^1S+6^1P+6^1D$ states; (+) present calculated GOSs for the 6^1S state; (×) present calculated GOSs for the 6^1D state. The experimental values (○) are obtained by subtracting the theoretical values (+) and (×) from the experimental values (●).

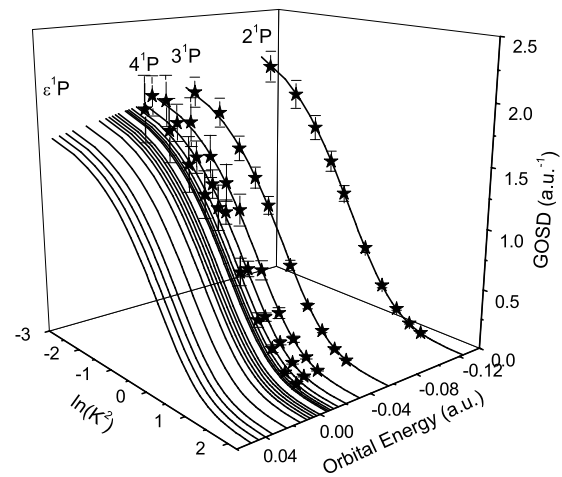


FIG. 9. The GOSD surface of the 1P channel. The experimental GOSDs of n^1P ($n=2,3,4,5,6$) states are obtained from the experimental values (○) in Figs. 1 and 5–8 by Eq. (10).

4^1S state. Our separated and total GOSs of n^1S , n^1P , and n^1D ($n=3,4,5,6$) states agree well with the previous theoretical results of Cann *et al.* [30]. Although there are no resolved experimental GOSs of n^1D excited states, which are smaller than those of the corresponding n^1S excited states but with the same order of magnitude, our calculated GOSs of n^1D states are anticipated to have the same accuracy as those of n^1S states since all the excited state wave functions are expanded on equal footing in the R -matrix method.

It can be found that the GOSs of n^1P states are larger than those of corresponding n^1D and n^1S states by about one or two orders. Therefore, the experimental GOSs of n^1P ($n=3,4,5,6$) states can be separated from the unresolved experimental GOSs [19] by subtracting the corresponding theoretical GOSs of n^1D ($n=3,4,5,6$) and n^1S ($n=5,6$) states. Our calculated GOSs of n^1P ($n=3,4,5,6$) states agree with the separated experimental data by about 5% as shown in Figs. 5–8. The available experimental GOSs of n^1P ($n=2,3,4,5,6$) states can be used to examine the calculated GOSD surface of the 1P channel as following.

As shown in Fig. 9, based on a few GOSD curves of n^1P and ε^1P states, the GOSD surface of the 1P channel is plotted, which is a smooth function of the excitation energies and $\ln K^2$. The available experimental GOSs of n^1P ($n=2,3,4,5,6$) states are transformed into GOSDs by Eq. (10). Our calculated GOSDs of n^1P ($n=2,3,4,5,6$) states agree with the available experimental results by about 5%. Therefore, the accuracy of this surface is examined since all the wave functions of the 1P channel are calculated in a unified manner in the R -matrix method. Similarly, as shown in Fig. 10, the GOSD surface of the 1S channel is tested by the experimental GOSDs of n^1S ($n=2,3,4$) states, which are obtained by the corresponding GOSs [19]. Our calculated GOSDs of n^1S ($n=2,3,4$) states agree with the experimental results by about 5% except two points of the 4^1S state. The differences may result from the experimental uncertainties. Our calculated GOSD surface of the 1D channel is shown in Fig. 11. Although there are no available resolved

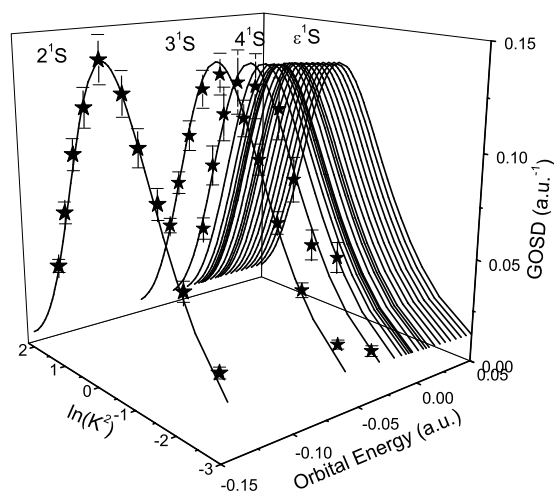


FIG. 10. The GOSD surface of the 1S channel. The experimental GOSDs of n^1S ($n=2,3,4$) states are obtained from the GOSs of Ref. [19] by Eq. (10).

experimental results of the 1D channel, it is anticipated that the surface of the 1D channel has the same accuracy as those of 1P and 1S channels. With the examined GOSD surfaces of 1S , 1P , and 1D channels with sufficient accuracy, the GOSDs (i.e., GOSs) of all n^1S , n^1P , and n^1D excited states can be obtained by surface spline interpolation [36] based on the benchmark points in the surfaces. Since the high-energy electron impact excitation differential cross sections (DCSs) are proportional to the GOSs as shown in Eq. (5), the DCSs of all the excited states can be readily obtained. This paper demonstrates the physical feature and feasibility to obtain the above infinite high-energy cross-section data. The detailed data, which should be useful in the relevant application fields, are too lengthy and beyond the scope of this paper, and will be reported elsewhere [37]. Therefore, the combination of the R -matrix method and QDT is an effective and accurate method to deal with the enormous high-energy electron impact excitation cross sections.

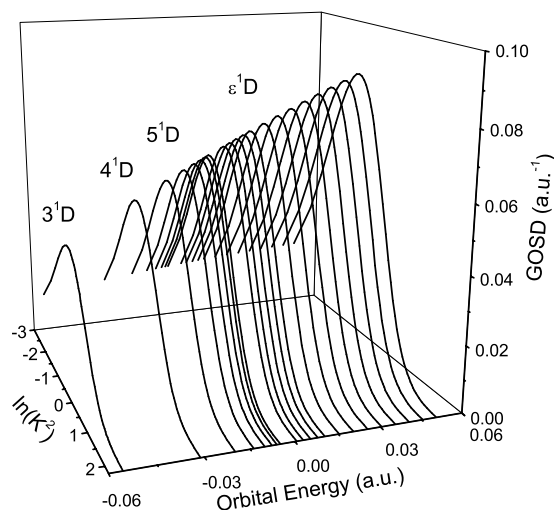


FIG. 11. The GOSD surface of the 1D channel.

III. CONCLUSION AND DISCUSSIONS

Using the modified R -matrix code, we calculate the GOSs of helium from the ground state to n^1S , n^1P , and n^1D ($n \rightarrow \infty$) and adjacent continuum excited states. In order to treat the bound-bound and bound-continuum transitions in a unified manner, the GOS density (GOSD) is defined based on the QDT. Our calculated GOSs of n^1S ($n=2,3,4$) and 2^1P states agree with the recent high-energy experimental results [19] by about 5% and agree well with the previous theoretical results [30] as shown in Figs. 1–4. Our calculated total GOSs of n^1P+n^1D ($n=3,4$) and $n^1S+n^1P+n^1D$ ($n=5,6$) states agree with the unresolved experimental results [19] by about 5% and agree well with the previous theoretical results [30] as shown in Figs. 5–8. Although there are no resolved experimental GOSs of n^1D excited states, our calculated GOSs of n^1D states are anticipated to have the same accuracy as those of n^1S states since all the excited-state wave functions are expanded on equal footing in the R -matrix method. Since the GOSs of n^1P states are larger than the GOSs of corresponding n^1D and n^1S states by about one or two orders, the experimental GOSs of n^1P ($n=3,4,5,6$) states can be separated from the unresolved experimental results [19] by subtracting the corresponding theoretical GOSs of n^1D and n^1S states. The available experimental GOSs of n^1P ($n=2,3,4,5,6$) and n^1S ($n=2,3,4$) states are used to test the accuracy of the GOSD surfaces. As shown in Figs. 9–11, the GOSD surfaces of 1S , 1P , and 1D channels are calculated and examined by the available experimental values. With the recommended GOSD surfaces with sufficient accuracy, the GOSDs (i.e., GOSs) of all n^1S , n^1P , and n^1D excited states can be obtained by surface spline interpolation [36,37]. Since the high-energy electron impact excitation differential cross sections (DCSs) are proportional to the GOSs, the DCSs of all these excited states can be readily obtained. Therefore, the combination of the R -matrix method and QDT is an effective and accurate way to deal with the enormous high-energy electron impact excitation cross sections for the ever-increasing needs in diverse relative fields.

Heretofore, we demonstrate how to deal with the high-energy electron impact excitation processes. The accuracy of the theoretical method and the modified code is tested stringently by the recent experiments [19]. Note that, from a point of view of partial wave expansions, the Born scattering amplitude f^B is the summation of infinite partial wave contributions as shown in Eq. (3), i.e., $f^B = \sum_{LS\pi} f_{LS\pi}^B$.

In practice, the incident energy of the impact electron can prevail over a wide range. In general, in the different energy regions, the different theoretical methods are applied. In the following, a scheme to deal with the intermediate- and low-energy collisions will be discussed. At low incident energies, the scattering amplitude f^I (i.e., the cross section) can be calculated by the R -matrix method with the same precision as that of f^B . More specifically, the target (e.g., the helium atom) and the impact electron should be treated as a collision complex, i.e., the $(N+1)$ -electron system, and the electron correlations can be considered by coupling the target wave functions with the impact electron wave functions. The scat-

tering amplitude f^l is a function of the incident energy E_i in addition to the momentum and energy transfers. With increasing incident energy E_i , the scattering amplitude converges to the Born scattering amplitude and becomes independent of E_i . The scattering amplitude f^l is also the summation of infinite partial wave contributions as shown by Eq. (1). However, at low incident energies, it is only necessary to calculate a few low partial wave contributions for the scattering amplitude f^l .

At intermediate incident energies, from a point of view of partial wave expansions, a large number of partial wave contributions should be calculated. Fortunately, as the angular momentum L increases, the exact partial scattering amplitude converges to the corresponding Born partial scattering amplitude [38]. The difference $f_{LS\pi}^C$ between the exact partial scattering amplitude and the Born partial scattering amplitude is

$$\begin{aligned}
 f_{LS\pi}^C &= f_{LS\pi}(\hat{k}') - f_{LS\pi}^B(\hat{k}') \\
 &= -\frac{\pi}{\sqrt{kk'}} \sum_{ij} \sum_{m_l m_{s_j}} \sum_{m_{s_i}} \sum_{\tilde{M}_L \tilde{M}_S} \sum_{\tilde{M}'_L \tilde{M}'_S} \sqrt{4\pi(2l_i+1)} Y_{l_j m_l}(\hat{k}') \\
 &\quad \times (T_{ji}^{LS\pi} - T_{ji}^{LS\pi(B)}) \times \langle \tilde{L}' \tilde{M}'_{\tilde{L}}, l_j m_l | LM_L \rangle \\
 &\quad \times \langle \tilde{S}' \tilde{M}'_{\tilde{S}}, s_j m_{s_j} | SM_S \rangle \langle LM_L | \tilde{L} \tilde{M}_{\tilde{L}}, l_i 0 \rangle \langle SM_S | \tilde{S} \tilde{M}_{\tilde{S}}, s_i m_{s_i} \rangle.
 \end{aligned} \tag{11}$$

Therefore, we can define an L_{\max} , beyond which all $f_{LS\pi}^C$ with $L \geq L_{\max}$ satisfy the relation $|f_{LS\pi}^C| < \delta$; δ is an appropriate convergence criterion. According to L_{\max} , all the partial wave contributions can be classified into two parts: one consists of infinite high partial scattering amplitudes with angular momentum $L \geq L_{\max}$, which are equal to the Born partial scattering amplitudes and can be calculated by the R -matrix method within the FBA; the other part consists of finite low partial scattering amplitudes with $L < L_{\max}$, which can also

be calculated by the R -matrix method. Therefore, at intermediate incident energies, the scattering amplitude f^l can be calculated by the R -matrix method within the FBA plus a correction term, i.e., $f^l = f^B + f^C$. Here the correction term f^C is the summation of $f_{LS\pi}^C$, i.e., $f^C = \sum_{S\pi, L=0}^{S\pi, L=L_{\max}} f_{LS\pi}^C$. Therefore, for the entire energy range the scattering amplitudes can be calculated by a unified formula: $f = f^B + f^C$; at high incident energies f^C is equal to zero, at intermediate incident energies f^C is the summation of $f_{LS\pi}^C$ with $L \leq L_{\max}$, and at low incident energies f is equal to f^l .

Similarly to the GOS, the apparent GOS (AGOS), i.e., $F^{\text{AG}}(E_i, \Delta E, K)$, for the low- and intermediate-energy impact processes can be defined, which is a function of the incident energies E_i , the energy transfers ΔE , and the momentum transfers K of the impact electron. With the increasing E_i , $F^{\text{AG}}(E_i, \Delta E, K)$ converges to the GOS, i.e., $F(\Delta E, K)$, and is independent of E_i . Similarly to the GOSD, the apparent GOSD (AGOSD), i.e., $dF^{\text{AG}}(E_i, \Delta E, K)/dE$, can be defined in the same way as that for the GOSD. According to the channel characters, the AGOSD for the intermediate-energy impact process is anticipated to be a smooth function of the excitation energies and the momentum transfers at a given incident energy. However, at low incident energies, the AGOSD is not a smooth function of ΔE and K because of the involvement of only a few partial wave amplitudes and the existence of resonances.

ACKNOWLEDGMENTS

This work is supported by the Ministry of Science and Technology and the Ministry of Education of China, the Key grant Project of the Chinese Ministry of Education (No. 306020), the National Natural Science Foundation of China, the National High-Tech ICF Committee in China, the Yin-He Super-computer Center, Institute of Applied Physics and Mathematics, Beijing, China, and the State Key Development Program for Basic Research of China (Grant No. 2001CB610508).

-
- [1] H. Bethe, *Ann. Phys.* **5**, 325 (1930).
 [2] M. Inokuti, *Rev. Mod. Phys.* **43**, 297 (1971).
 [3] B. G. Tian and J. M. Li, *Acta Phys. Sin.* **33**, 1401 (1984).
 [4] X. C. Pan and J. M. Li, *Acta Phys. Sin.* **34**, 1500 (1985).
 [5] X. Y. Han, L. Voky, and J. M. Li, *Chem. Phys. Lett.* **21**, 54 (2004).
 [6] X. L. Liang, X. C. Pan, and J. M. Li, *Chem. Phys. Lett.* **2**, 545 (1985).
 [7] U. Fano, *J. Opt. Soc. Am.* **65**, 979 (1975).
 [8] M. J. Seaton, *Rep. Prog. Phys.* **46**, 167 (1983).
 [9] J. M. Li, *Acta Phys. Sin.* **29**, 419 (1980).
 [10] L. Liu and J. M. Li, *J. Phys. B* **24**, 1893 (1991).
 [11] P. G. Burke, A. Hibbert, and W. D. Robb, *J. Phys. B* **4**, 153 (1971).
 [12] K. A. Berrington, P. G. Burke, J. J. Chang, A. T. Chivers, W. D. Robb, and K. T. Taylor, *Comput. Phys. Commun.* **8**, 149 (1971).
 [13] K. A. Berrington, P. G. Burke, M. L. Dourneuf, W. D. Robb, K. T. Taylor, and L. Voky, *Comput. Phys. Commun.* **14**, 346 (1978).
 [14] K. A. Berrington, P. G. Burke, K. Butler, M. J. Seaton, P. J. Storey, K. T. Taylor, and Y. Yan, *J. Phys. B* **20**, 6379 (1987).
 [15] L. VoKy, H. E. Saraph, W. Eissner, Z. W. Liu, and H. P. Kelly, *Phys. Rev. A* **46**, 3945 (1992).
 [16] K. A. Berrington and A. E. Kingston, *J. Phys. B* **20**, 6631 (1987).
 [17] K. A. Berrington, W. B. Eissner, and P. H. Norrington, *Comput. Phys. Commun.* **92**, 290 (1995).
 [18] K. Z. Xu, R. F. Feng, S. L. Wu, Q. Ji, X. J. Zhang, Z. P. Zhong, and Y. Zheng, *Phys. Rev. A* **53**, 3081 (1996).
 [19] X. J. Liu, L. F. Zhu, Z. S. Yuan, W. B. Li, H. D. Cheng, J. M. Sun, and K. Z. Xu, *J. Electron Spectrosc. Relat. Phenom.* **135**, 15 (2004).
 [20] A. Messiah, *Quantum Mechanics* (North-Holland, Amsterdam,

- 1973).
- [21] H. Bethe, Z. Phys. **76**, 293 (1932).
- [22] C. M. Lee (Jia-Ming Li), Phys. Rev. A **10**, 1598 (1974).
- [23] U. Fano and C. M. Lee (Jia-Ming Li), Phys. Rev. Lett. **31**, 1573 (1973).
- [24] A. Hibbert, Comput. Phys. Commun. **9**, 141 (1975).
- [25] J. Yan, Y. Z. Qu, L. VoKy, and J. M. Li, Phys. Rev. A **57**, 997 (1998).
- [26] Y. L. Peng, M. S. Wang, X. Y. Han, and J. M. Li, Chem. Phys. Lett. **8**, 56 (2004).
- [27] Y. L. Peng, M. S. Wang, X. Y. Han, and J. M. Li, J. Phys. B **38**, 3825 (2005).
- [28] C. L. Pekeris, Phys. Rev. **126**, 1470 (1962).
- [29] J. M. Li, L. V. Ky, Y. Z. Qu, J. Yan, P. H. Zhang, H. L. Zhou, and P. Faucher, Phys. Rev. A **55**, 3239 (1997).
- [30] N. M. Cann and J. A. Thakkar, J. Electron Spectrosc. Relat. Phenom. **123**, 143 (2004).
- [31] M. A. Dillon and E. N. Lassette, J. Chem. Phys. **62**, 2373 (1975).
- [32] D. C. Cartwright, G. Csanak, S. Trajmar, and D. F. Register, Phys. Rev. A **45**, 1602 (1992).
- [33] Z. P. Zhong, R. F. Feng, S. L. Wu, L. F. Zhu, X. J. Zhang, and K. Z. Xu, J. Phys. B **30**, 5305 (1997).
- [34] T. Y. Suzuki, H. Suzuki, F. J. Currell, S. Ohtani, Y. Sakai, T. Takayanagi, and K. Wakiya, Phys. Rev. A **57**, 1832 (1998).
- [35] A. Pochat, D. Rozuel, and J. Peresse, J. Phys. (Paris) **34**, 701 (1973).
- [36] P. Dierckx, *Curve and Surface Fitting with Splines*, (Oxford University Press, New York, 1993).
- [37] X. Y. Han *et al.* (unpublished).
- [38] X. Pan, Phys. Rev. Lett. **66**, 2972 (1991).